Pergamon

Int. J. Solids Structures Vol. 32, No. 3/4, pp. 329–340, 1995

0020–7683/95 $9.50 + .00

0020–7683(94)00127–8

CONTACT MECHANICS OF HERTZIAN CONE CRACKING

S. Y. CHEN†, T. N. FARRIS† and S. CHANDRASEKAR‡
School of Aeronautics and Astronautics† and School of Industrial Engineering‡,
Purdue University, West Lafayette, IN 47907-1282, U.S.A.

(*Received* 23 *June* 1994)

Abstract—Quasi-static indentation of brittle materials with a spherical indenter produces Hertzian cone cracks. The variation of cone crack length with load is measured by indenting soda-lime glass blocks with a 3.17 mm diameter hardened steel ball and photographing the cracks through a side face of the blocks. Assuming that the contact pressure distribution is Hertzian, axisymmetric boundary elements are used to accurately calculate stress intensity factors along the front of the cone crack by adapting the modified crack closure integral. The boundary element results are verified through comparisons with finite element calculations and prior results in the literature. The Mode I stress intensity factor is found to be a positive monotonically decreasing function of cone crack length, provided that the contact radius is not greater than the cone crack radius at the surface. Calculations using the Hertzian pressure distribution predict that the cone crack will arrest when the contact radius is greater than the cone crack length at the surface. However, experimental observations suggest that as the contact radius approaches the cone crack radius at the surface, interaction effects lead to a non-Hertzian pressure distribution. Detailed finite element contact mechanics of the actual cracked body are used to show that the contact pressure is singular at the edge of contact once the contact radius becomes equal to the cone crack radius. Furthermore, cone crack growth continues even when contact between the indenter and the cracked body occur outside of the cracked region, which is consistent with experimental observations. This latter aspect of cone crack growth cannot be predicted on the basis of a Hertzian pressure distribution.

1. INTRODUCTION

Indentation fracture of brittle materials generated by spherical and pointed (i.e. cone, Vickers, Knoop) indenters has been the focus of much research. Interest in this problem stems from the role of indentation-induced flaws in controlling the strength of brittle solids, and from the use of indentation techniques to measure fracture surface energy and fracture toughness of brittle solids. In addition there is recent evidence that indentation fracture can be used to model material removal during finishing of ceramics (Chauhan *et al.*, 1993). Indentation by spheres is commonly referred to as Hertzian indentation after Hertz, who originally calculated the relevant pressure distribution under the indenter. Hertzian indentation of brittle materials leads to Hertzian ring and cone cracking. Figure 1 describes the

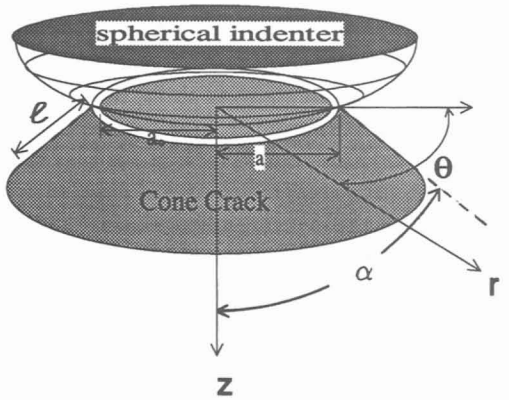

Fig. 1. Schematic view of cone cracking showing spherical steel indentation of glass block; cone crack length l; half-apex angle, α; Hertz contact radius, a_0; cone crack radius at surface, a.

typical Hertzian cone crack geometry and defines the following parameters: cone crack length, l; half-apex angle, α; cone crack radius at the surface, a (ring crack radius); and contact radius calculated using the Hertzian assumptions, a_0. The term "ring crack" describes the circularly shaped crack that initially forms at this surface and which after a small amount of growth perpendicular to the surface, 'pops' into the well-developed cone crack. Hertzian indentation of brittle materials and the cone cracks that it produces are the focus of this paper.

Tillett (1956) and Roesler (1956a,b) detail numerous historical observations of ring cracking being visible once the surface tensile stress is much greater than that required for fracture in bulk tensile test specimens. This has been attributed to the small volume acted upon by the contact-induced tensile stress. While the maximum tensile stress induced by frictionless Hertzian contact is known to occur just at the edge of the contact patch, ring cracks have been observed to form outside of the radius of contact predicted by Hertz (Tillett, 1956; Chaudhri and Yoffe, 1981). Also, it has been observed experimentally when indenting fused silica and sapphire with hard spheres that the contact radius is greater than that predicted by Hertz (Chaudhri and Yoffe, 1981). Johnson *et al.* (1973) have shown from a stress analysis, which considered the elasticity of the indenter, that the actual location of the maximum tensile stress indeed may lie just outside the contact patch.

Frank and Lawn (1967) investigated the development of the cone crack from the ring crack in the strongly inhomogeneous Hertzian stress field. They approximately calculated the Mode I stress intensity factor at the cone crack front by modeling it as a two-dimensional plane strain crack in an infinite medium loaded by the stresses acting on the location of the cone crack in the corresponding uncracked body. It was assumed that the inclined sides of the cone crack followed trajectories of the minimum principal stress so that it was perpendicular to the maximum principal stress. This model predicts that the crack propagation arrests at a depth which is related to the applied load.

Warren (1978) used a similar two-dimensional approximation and considered the effect of ring crack initiation some distance outside of the circle of contact. The model was combined with experiments to measure the fracture toughness of carbides based on the initiation of the ring crack. Warren (1978) concluded that the reliability of interpretation could be improved by a more sophisticated fracture mechanics analysis. Mouginot and Maugis (1985) also used the two-dimensional approximation to analyze cracks generated by both spheres and flat punches. Zeng *et al.* (1992) combined a similar approach with measurements to obtain the fracture toughness of soda lime glass and obtain values that are load independent and reasonably consistent with values for K_{Ic} determined by other means. None of the above analyses included the effect of the actual crack shape and its interrelation with the free surface in the calculation of the stress intensity factors.

The mixed mode stress intensity factors for the Hertzian cone crack subjected to Hertzian contact pressures have been fully analyzed numerically only recently by Yingzhi and Hills (1991). A global–local finite element method was used, and effects of the free surface and the curved nature of the crack front were included in the analysis. Yingzhi and Hills (1991) found that the mode II stress intensity factor was about one tenth of the mode I stress intensity factor. Recent boundary element calculations by Chen *et al.* (1993) have yielded stress intensity factors within 3% of the FEM calculations of Yingzhi and Hills (1991). These stress intensity factor calculations show that when the contact pressure is applied to a patch of radius larger than the radius of the cone crack at the surface, the mode I stress intensity factor is zero and cone crack growth is arrested.

In the present study, soda-lime glass blocks are indented with a hardened steel sphere. The variation of the cone crack length with applied load is determined experimentally by observing the blocks through their sides while the load is still applied. The predicted variation of cone crack length with applied load, calculated by assuming that the Hertzian pressure distribution remains unaffected by the presence of the crack, is compared with the experimental measurements. The comparison shows that the pressure distribution is non-Hertzian for fully developed cone cracks. This result motivates the following finite element calculations that detail the actual pressure distribution, which is then used to predict the variation of cone crack length with load. The analysis shows that when the contact radius

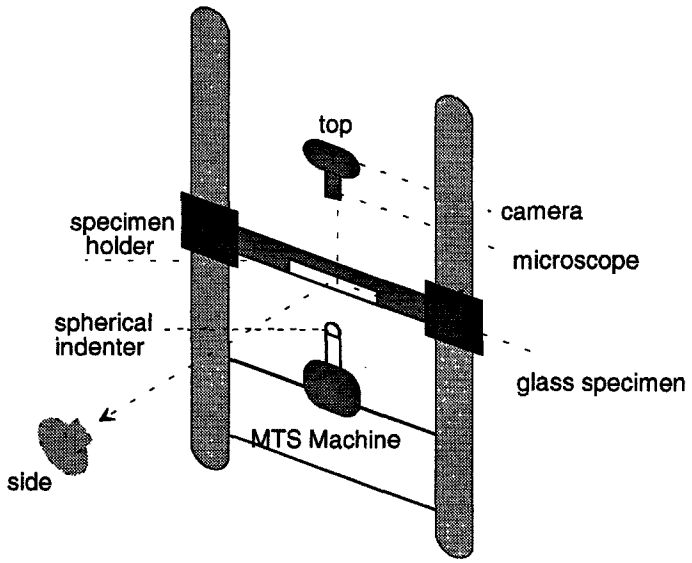

Fig. 2. Schematic of *in situ* observation of indentation cracking.

predicted by Hertz is larger than the cone crack radius at the surface, the load is carried in part by the resulting singularity in the contact pressure at the edge of contact. Indeed, the order of such singularities was investigated in detail by Professor Dundurs (Dundurs and Lee, 1972) who showed that it could be written explicitly in terms of Dundurs' parameters. As the load is increased further it is found that contact also occurs just outside of the cracked region and the cone crack continues to grow.

2. EXPERIMENTAL DETAILS

Soda-lime glass blocks, $5 \times 5 \times 1.25$ cm and devoid of residual stress, were indented by a hardened steel sphere of diameter 3.17 mm. The relevant mechanical properties (typical values) for these materials were: Young's modulus, $E = 200$ GPa, and Poisson's ratio, $\nu = 0.25$, for steel; $E = 69$ GPa, $\nu = 0.23$, tensile strength, $\sigma_F = 100$ MPa, and fracture toughness, $K_{Ic} = 0.75$ MPa $\sqrt{\text{m}}$ for soda-lime glass. The blocks were polished to an optical surface quality prior to indentation.

In a typical indentation experiment, the indenter, which was attached to the cross-head of an MTS testing machine (MTS model 458.20), was loaded against the 1.25×5 cm face of the block. The cross-head speed when indenting the glass block was 0.1 mm min^{-1}. During loading and unloading, the indenter and the block were observed using an optical microscope and photographed through the top and side faces of the block, see Fig. 2. Particular attention was paid to observing the evolution of the cone crack length as the indenter load was increased.

From microscopic observations and photographs of the cone crack (see Fig. 3) and measurements of the indenter load, the variation of cone crack length with applied load was determined (Fig. 4). The cone crack length was found to increase monotonically with the applied load.

A photograph of the top view of the cone crack taken after the indenter was unloaded is shown in Fig. 5. The axisymmetric geometry and loading leads to the assumption that the fully developed cone crack grows in a self-similar manner, thereby allowing for an axisymmetric analysis. In all likelihood, the ring crack initiates at a point flaw which is most certainly not axisymmetric and grows quickly into an axisymmetric shape due to the axisymmetric stress field. The following analysis concerns self-similar growth following formation of an axisymmetric ring crack and its "pop-in" into a well-developed cone crack.

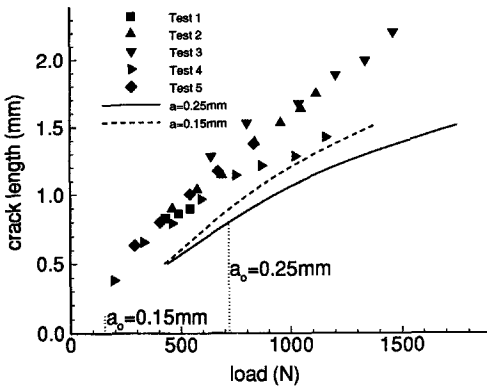

Fig. 4. Experimental and predicted cone crack length for 3.17 mm (0.125 in) ball indentation on glass using $\alpha = 62°$.

3. ANALYSIS

3.1. *Finite element details*

The finite element calculations are performed with ANSYS.† A combination of three-noded triangular and four-noded quadrilateral axisymmetric elements are used to model both the steel indenter and the glass specimen. The lower half of the indenter is modeled with loads applied through vertically displacing the horizontal diametrical circle. The total number of elements used depends on the cone crack length, radius and angle, as well as upon the indenter radius. Approximately 2000 elements were used for each material body. A typical complete finite element mesh and details of the near contact are shown in Figs 6 and 7.

Axisymmetric, frictionless point-to-surface contact elements are used to model the interaction between the lower surface of the indenter and the top surface of the specimen. These elements require one node on the surface of one body and two nodes on the surface of the remaining body. The contact elements ensure that the contact pressure is positive inside the contact patch and zero outside of contact and that there is no interpenetration of the two bodies. The applied load is simulated by gradually increasing the uniform displacements along the top boundary of the half-spherical indenter. The contact radius, i.e. the radius of the projected circle over which the indenter and block are in contact, is calculated through iteration at each load step. The iterative procedure assumes a contact radius and calculates the contact pressure, regions of assumed contact having negative pressure are removed from contact, and regions outside of contact exhibiting interpenetration are added to contact before the next iteration. Convergence on the contact radius occurs once all inequalities are satisfied. Similar contact elements are used between the faces of the crack to inhibit interpenetration.

The strain energy release rate, defined as the energy released per unit area of crack growth, is given by

$$G_{\mathrm{I}} = \lim_{\Delta A \to 0} \frac{1}{2\Delta A} \int_{\Delta A} (u_{\mathrm{n}}^{+} - u_{\mathrm{n}}^{-})\, \sigma_{\mathrm{n}} \mathrm{d}A \tag{1}$$

$$G_{\mathrm{II}} = \lim_{\Delta A \to 0} \frac{1}{2\Delta A} \int_{\Delta A} (u_{\mathrm{t}}^{+} - u_{\mathrm{t}}^{-})\, \tau_{\mathrm{t}} \mathrm{d}A, \tag{2}$$

where G_{I} and G_{II} are the mode I and mode II strain energy release rates, respectively, ΔA is the crack extension area, $(u_{\mathrm{n}}^{+} - u_{\mathrm{n}}^{-})$ and $(u_{\mathrm{t}}^{+} - u_{\mathrm{t}}^{-})$ are the total normal and tangential crack opening displacements, respectively, and σ_{n} and τ_{t} are the normal and shear stresses ahead of the crack.

† ANSYS, a product of Swanson Analysis Systems, Inc., Houston, PA, was made available through an academic license to Purdue University.

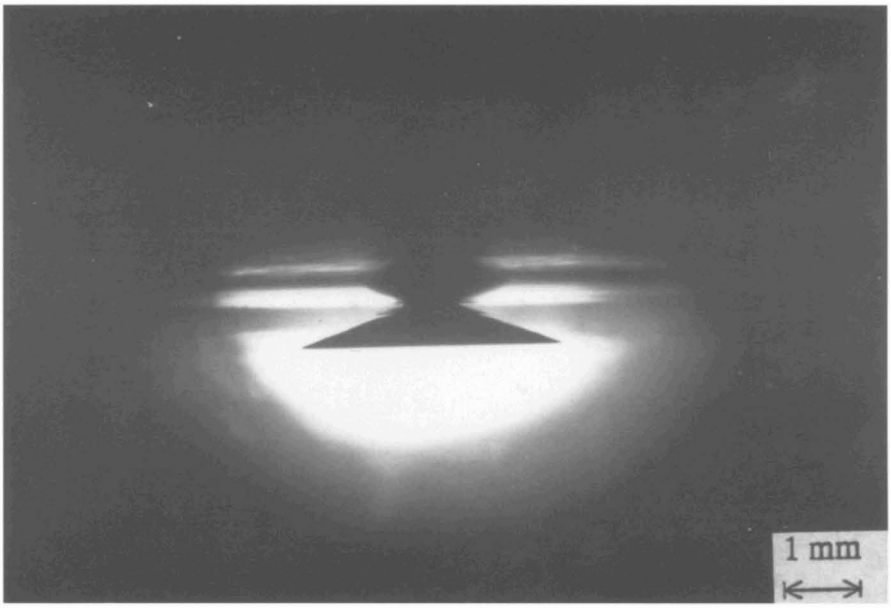

Fig. 3. Side view of cone crack in soda-lime glass.

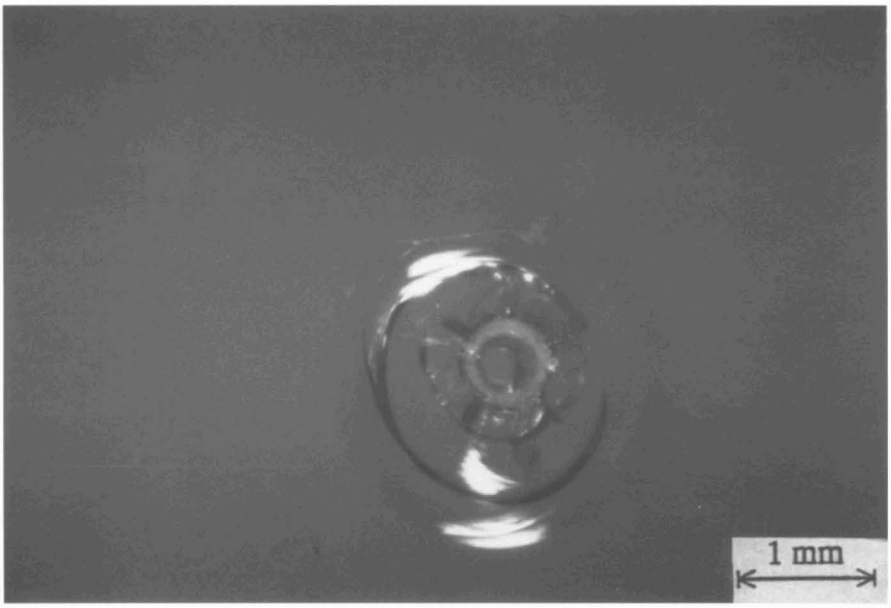

Fig. 5. Top view of cone crack in soda-lime glass.

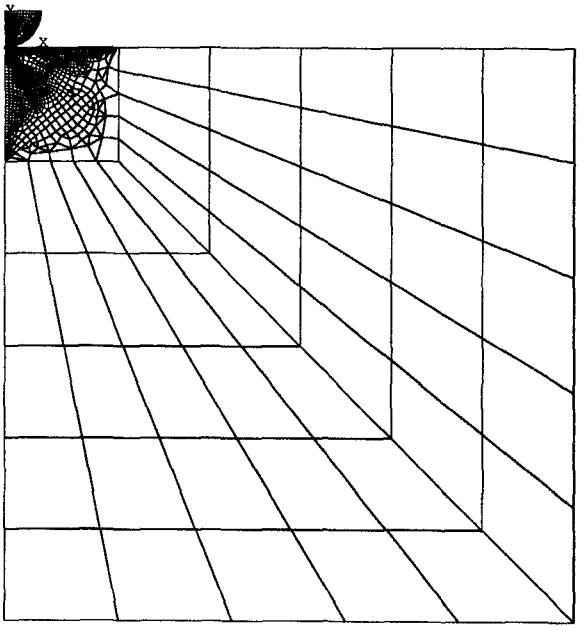

Fig. 6. Finite element mesh.

Strictly speaking, the stresses, σ_n and τ_t are those existing ahead of the crack tip before crack extension and the displacements are those behind the crack tip after crack extension, so that the products in eqns (1) and (2) are taken for quantities at exactly the same position in space. The exact evaluation of eqns (1) and (2) requires FEM data for two different crack lengths. However, since the displacements just behind the crack tip both before and after a small crack extension are almost equal, eqns (1) and (2) can be approximated by using the stresses and displacements for one crack length. This approximation, known as the modified crack closure integral, has been used successfully in two-dimensional finite elements (Rybicki and Kanninen, 1977) and boundary elements (Farris and Liu, 1993).

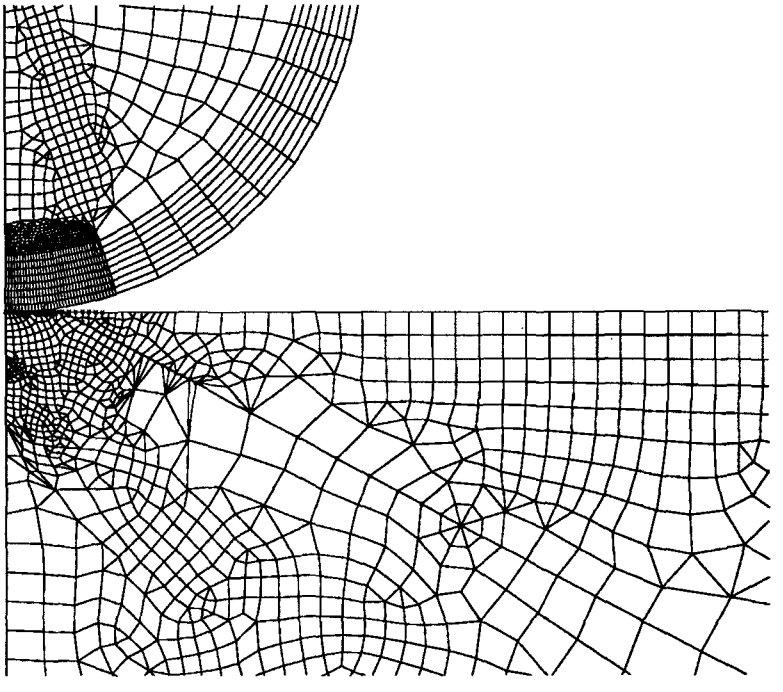

Fig. 7. Finite element mesh near contact.

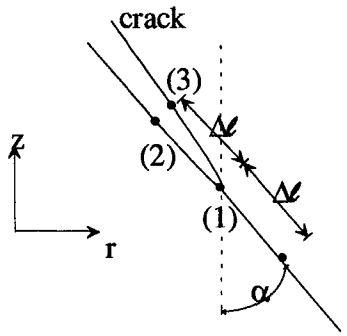

Fig. 8. Nodes and elements near the crack tip used in modified crack closure integral.

The modified crack closure integral is evaluated using four-node finite elements in terms of nodal displacements and forces as

$$G_{\mathrm{I}} = \frac{1}{2\Delta A}(u_{\mathrm{n}}^3 - u_{\mathrm{n}}^2)\, F_{\mathrm{n}}^1 \tag{3}$$

$$G_{\mathrm{II}} = \frac{1}{2\Delta A}(u_{\mathrm{t}}^3 - u_{\mathrm{t}}^2)\, F_{\mathrm{t}}^1, \tag{4}$$

where the superscripts refer to the nodal values illustrated in Fig. 8, and F_{n} and F_{t} are the normal and tangential nodal forces respectively, due to elements on one side of the line containing the crack. Finally, stress intensity factors are calculated from the strain energy release rates as

$$K_{\mathrm{I}} = \sqrt{\frac{G_{\mathrm{I}}E}{1-\nu^2}}, \quad K_{\mathrm{II}} = \sqrt{\frac{G_{\mathrm{II}}E}{1-\nu^2}}. \tag{5}$$

3.2. *Stress intensity factors due to applied pressure*

The FEM stress intensity factor calculation is validated through comparison with previous results of Yingzhi and Hills (1991). For this calculation, the loading is taken as a Hertzian contact pressure distribution given by

$$\sigma_z(r,0) = -p_0\sqrt{1-\frac{r^2}{a_0^2}}, \tag{6}$$

where

$$p_0 = \frac{3P}{2\pi a_0^2}, \quad a_0 = \left(\frac{3PR}{4E^*}\right)^{1/3}, \quad \frac{1}{E^*} = \frac{1-\nu_{\mathrm{g}}^2}{E_{\mathrm{g}}} + \frac{1-\nu_{\mathrm{s}}^2}{E_{\mathrm{s}}},$$

R is the radius of the indenter, a_0 is the radius over which the pressure is applied (recall Fig. 1), and the subscripts s and g refer to steel and glass, respectively. Figure 9 shows the calculated stress intensity factors obtained using the present FEM results with the modified crack closure integral, as well as the global–local FEM results of Yingzhi and Hills (1991). The two results differ by less than 3%. Chen *et al.* (1993) have also recently used axisymmetric boundary element calculations to validate the present FEM results.

The cone crack angle used in Fig. 9 is within the range of angles commonly observed in experiment. Many investigations have assumed that the crack grows perpendicular to the maximum principal stress corresponding to Hertz contact in the uncracked media. These trajectories predict that the initial ring crack would form perpendicular to the surface before turning to grow at an angle into a cone crack. Since the length of growth

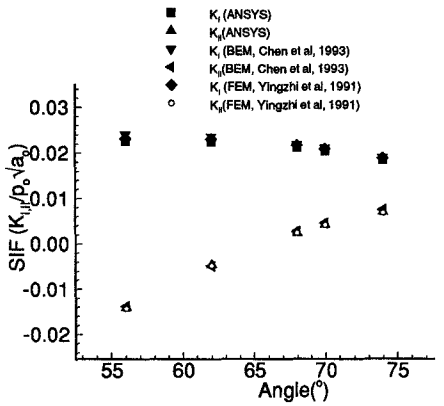

Fig. 9. Stress intensity factors for cone crack subjected to a Hertzian pressure distribution, $l/a_0 = 1$, $a/a_0 = 1.05$.

perpendicular to the surface is usually small, the cone crack has been modeled as growing along a straight line, which is inclined at an angle of 62° with the normal to the surface. The largest tensile stress in the body occurs just at the edge of contact such that

$$\sigma_r(a_0, 0) = \frac{1-2\nu}{3} p_0 . \tag{7}$$

In many instances, ring cracks are observed to occur when this stress is as high as 10 times the manufacturer's reported values of 100 MPa for the tensile strength of soda-lime glass blocks. Hence, as the load is applied, ring cracks should occur just at the edge of contact. However, Johnson *et al.* (1973) have shown from a stress analysis, which includes the effect of indenter elasticity, that the location of the maximum stress may occur just outside of the contact such that $r > \sim a, z = 0$. This is consistent with some observations of the location of ring crack occurrence (Zeng *et al.*, 1992). As the crack follows the stress trajectory during growth, it will continue to have a positive mode I stress intensity factor.

Chen *et al.* (1993) used boundary elements to quantify one feature of the growth of the ring/cone crack system that one might assume using knowledge of the subsurface Hertzian stress field. When a ring crack forms at the surface and does not propagate into a well-developed cone crack, then as the indenter load is increased, the ring crack eventually will be encompassed within the circle of contact. This is based on the assumption that the presence of the ring/cone crack does not affect the pressure distribution. Under such conditions, the stress intensity factor calculation illustrated in Fig. 10 shows that the growth of the ring crack into the sub-surface will be arrested. The negative mode I stress intensity factors are physically not realistic, but indicate that for this configuration the crack would close and crack growth would be arrested. The results in Fig. 10 also illustrate that for a

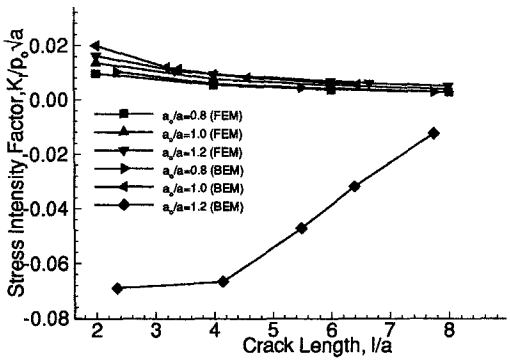

Fig. 10. Normalized stress intensity factors for Hertzian cone cracking, $\alpha = 62°$, $\nu = 0.23$, $a = 0.25$ mm. The FEM curves are for the contact problem while the BEM curves taken from Chen *et al.* (1993) are for the corresponding Hertzian pressure distribution.

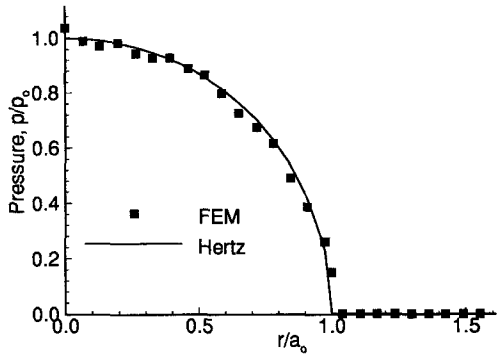

Fig. 11. Contact pressure distribution for Hertzian contact (no cone crack) $P = 754$ N, $\mathring{a}_0 = 0.254$ mm.

given contact size, the stress intensity factor decreases with increasing cone crack length when the ring crack size is larger than the contact size.

4. THE CONTACT PROBLEM

Experimental observations (Tillett, 1956; Benbow, 1960) indicate that the cone crack continues to grow under increasing load even when the contact radius, as predicted by a Hertzian analysis of the uncracked solid, is greater than the radius of the cone crack at the surface. This contradicts the prediction of the stress intensity factor calculation of the previous section, which suggests that the crack should stop growing once the contact radius exceeds the radius of the cone crack at the surface. It is this fact that motivated the present contact mechanics analysis of Hertzian cone cracking.

The contact problem to be solved is shown in Figs 1 and 6. A cone crack of length l, semi apex angle α, and radius at the surface a is assumed to exist in the glass block. The steel ball is brought into contact with the glass block by incrementally displacing its horizontal diametrical circle. A 3.17 mm diameter ball is used in all of the FEM calculations. The contact radius, contact pressure distribution, and total applied load is calculated at each increment. The total load is calculated by summing the nodal forces for nodes in contact. Accuracy of the contact elements and accompanying algorithm is assessed by first removing the cone crack. Results for this case are compared to Hertzian theory (eqn 6) in Fig. 11. The contact pressure calculated on the surface of the sphere by ANSYS is reported except where the nodal forces are zero, at which location the pressure is reported as zero. The excellent agreement between FEM and Hertz theory (Fig. 11) provides confidence for the following calculations.

Cone crack radii at the surface used as inputs to the finite element program were chosen in the range of experimentally estimated radii (0.15–0.25 mm). These radii are difficult to measure accurately, in part due to the damage caused by the indentation illustrated in Fig. 5. The half-apex angle (α) of the cone crack is taken as 62° in the finite element model.

The solution to the full contact problem is illustrated through the example shown in Figs 12–14. Figure 12 shows a case in which the contact radius is less than the radius of the cone crack at the surface. Note that the pressure distribution is well approximated by the Hertzian pressure distribution given by eqn (6). Figure 13 corresponds to a case in which the contact load is just large enough for the contact radius to equal the radius of the cone crack at the surface, while Fig. 14 illustrates a case in which the load is increased well beyond the value for which the contact radius is equal to the radius of the cone crack. Note the singular nature of the pressure distribution at the edge of contact in Fig. 14. This pressure distribution is significantly different from that calculated assuming a Hertzian pressure distribution. The stress intensity factors corresponding to the full solution to the contact problem are shown in Fig. 10. In particular it can be seen that when the Hertzian

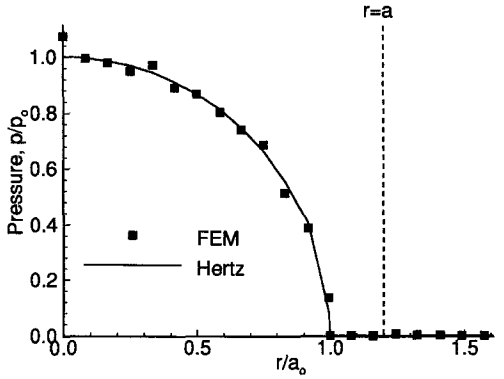

Fig. 12. Contact pressure distribution including cone crack interaction effects $P = 368$ N, $a_0 = 0.200$ mm, $a = 0.250$ mm, $l = 2$ mm.

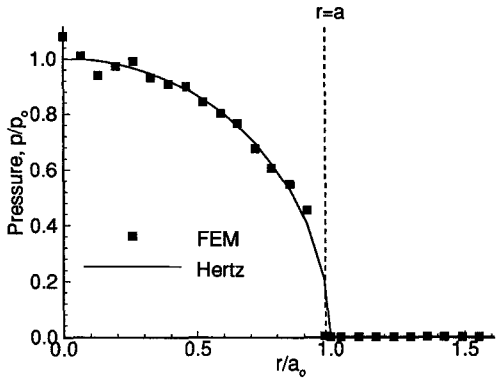

Fig. 13. Contact pressure distribution including cone crack interaction effects $P = 754$ N, $a_0 = 0.255$ mm, $a = 0.250$ mm, $l = 2$ mm.

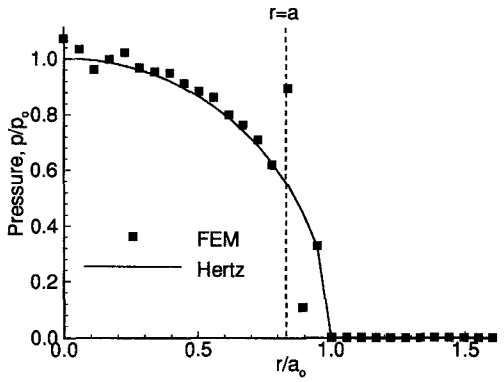

Fig. 14. Contact pressure distribution including cone crack interaction effects $P = 1200$ N, $a_0 = 0.297$ mm, $a = 0.25$ mm, $l = 2$ mm.

contact radius is greater than the cone crack radius at the surface, the contact problem yields positive stress intensity factors, while the Hertzian pressure distribution does not.

The above interaction between the cone crack and the contact pressure distribution is to our knowledge unreported in the literature. Previous investigations which have assumed a Hertzian pressure distribution conclude that the cone crack will cease to grow once the contact radius exceeds the radius of the cone crack at the surface (Lawn, 1993). However, the finite element calculations clearly show that the pressure distribution deviates from the Hertzian distribution as the contact radius reaches the cone crack radius at the surface. Furthermore, cone crack growth continues even when contact occurs outside the cracked region. Thus the cone crack will continue to grow stably as the load is increased, a fact which is consistent with experimental observations.

If it is assumed that crack growth occurs when the stress intensity factor is greater than the fracture toughness, then the cone crack length can be predicted as a function of load. The predicted values using the full contact problem solution are shown in Fig. 4 for different assumed radii of the cone crack at the surface. The predicted values are reasonably close to those measured experimentally. Since the radius of the surface trace of the ring/cone crack is difficult to measure experimentally, the predictions are made for a range of these radii. It is found that the predicted crack length decreases as the radius of the cone crack at the surface increases. The different estimates of the ring crack radius do not significantly change the prediction of the cone crack length.

5. CONCLUSION

The relationship between the Hertzian cone crack length and the indentation load in soda-lime glass has been measured and predicted using axisymmetric finite elements. The full solution to the contact problem shows that there are singularities in the pressure distribution when the contact radius reaches or exceeds the cone crack radius at the surface. Moreover, cone crack growth continues even when contact occurs outside of the cracked region. The estimated cone crack length vs load relationship reasonably agrees with experimental values for the load range in which the cone crack is fully developed. The assumption of the initial ring crack radius has only a small effect on the stress intensity factor calculation. Thus, the elastic contact problem that includes the interaction between the cone crack and the contact pressure accurately predicts cone crack growth over a wide load range.

In summary, the main conclusion of this paper is that the interaction between cone cracking and the contact pressure distribution must be included to explain the growth of fully developed cone cracks.

Acknowledgment—This research is supported in part by the National Science Foundation through grants MSS9057082, Dr J. Larsen-Basse, Program Director and DDM 9057916, Dr K. Srinivasan, Program Director.

REFERENCES

Benbow, J. J. (1960). Cone cracks in fused silica. *Proc. Phys. Soc. B* **72,** 697–699.

Chaudhri, M. M. and Yoffe, E. H. (1981). The area of contact between a small sphere and a flat surface. *Phil. Mag.* **44**(3), 667–675.

Chauhan, R., Ahn, Y., Chandrasekar, S. and Farris, T. N. (1993). Role of indentation fracture in free abrasive machining of ceramics. *Wear* **162,** 246–257.

Chen, S. Y., Farris, T. N. and Chandrasekar, S. (1993). Experimental and boundary element analysis of Hertzian cone cracking. In *Proc. Symp. Fatigue and Fracture of Aerospace Structural Materials*, ASME: AD Vol. 36, pp. 135–150.

Dundurs, J. and Lee, M. S. (1972). Stress concentration at a sharp edge in contact problems. *J. Elast.* **2**(2), 109–112.

Farris, T. and Liu, M. (1993). Boundary element crack closure calculation of three dimensional stress intensity factors. *Int. J. Fract.* **60**(1), 33–47.

Frank, F. C. and Lawn, B. R. (1967). On the theory of Hertzian fracture. *Proc. R. Soc. Ser. A* **299,** 291–306.

Johnson, K. L., O'Connor, J. J. and Woodward, A. C. (1973). The effect of indenter elasticity on the Hertzian fracture of brittle materials. *Proc. R. Soc. Ser. A* **334,** 95–117.

Lawn, B. R. (1993). *Fracture of Brittle Solids.* 2nd edn, Chap. 9, p. 253. Cambridge University Press, Cambridge.

Mouginot, R. and Maugis, D. (1985). Fracture indentation beneath flat and spherical punches. *J. Mater. Sci.* **20,** 4354–4376.

Roesler, F. C. (1956a). Brittle fractures near equilibrium. *Proc. Phys. Soc. B* **69,** 981–992.

Roesler, F. C. (1956b). Indentation hardness of glass as an energy scaling law. *Proc. Phys. Soc. B* **69,** 55–60.

Rybicki, E. F. and Kanninen, M. F. (1977). A finite element calculation of stress intensity factors by a modified crack closure integral. *Engng Fract. Mech.* **9,** 931–938.

Tillett, J. P. A. (1956). Fracture of glass by spherical indenters. *Proc. Phys. Soc. B* **69,** 47–54.

Warren, R. (1978). Measurement of the fracture properties of brittle solids by Hertzian indenters. *Acta Metall.* **46,** 1759–1769.

Yingzhi, L. and Hills, D. (1991). The Hertzian cone crack. *J. Appl. Mech.* **58**(1), 120–127.

Zeng, K., Breder, K. and Rowcliffe, D. J. (1992). The Hertzian stress field and formation of cone cracks: I. theoretical approach; II. determination of fracture toughness. *Acta Metall. Mater.* **40**(10), 2595–2605.